Mon. Not. R. Astron. Soc. **393,** 798–807 (2009) doi:10.1111/j.1365-2966.2008.14229.x

Hubble Space Telescope survey of the Perseus cluster – II. Photometric scaling relations in different environments

S. De Rijcke,[1⋆] S. J. Penny,[2] C. J. Conselice,[2] S. Valcke[1] and E. V. Held[3]

[1] *Sterrenkundig Observatorium, Universiteit Gent, Krijgslaan 281, S9, B-9000 Gent, Belgium*
[2] *School of Physics and Astronomy, University of Nottingham, Nottingham NG7 2RD*
[3] *Osservatorio Astronomico di Padova, INAF, vicolo dell'Osservatorio 5, 35122 Padova, Italy*

Accepted 2008 November 10. Received 2008 October 13; in original form 2008 July 4

ABSTRACT

We investigate the global photometric scaling relations traced by early-type galaxies in different environments, ranging from dwarf spheroidals, over dwarf elliptical galaxies (dEs), up to giant ellipticals ($-8\,\mathrm{mag} \gtrsim M_V \gtrsim -24\,\mathrm{mag}$). These results are based, in part, on our new *Hubble Space Telescope* (*HST*)/Advanced Camera for Surveys (ACS) F555W and F814W imagery of dwarf spheroidal galaxies in the Perseus cluster. The full sample, built from our *HST* images and from data taken from the literature, comprises galaxies residing in the Local Group; the Perseus, Antlia, Virgo and Fornax clusters; and the NGC 5898 and NGC 5504 groups.

Photometric parameters, such as the half-light radius, the central surface brightness and the Sérsic exponent n, are used to parametrize the light distributions and sizes of early-type galaxies. All these parameters vary in a continuous fashion with galaxy luminosity over a range of more than six orders of magnitude in luminosity. We also find that all early-type galaxies follow a single colour–magnitude relation (CMR), which we interpret as a luminosity–metallicity relation for old stellar populations. These scaling relations are almost independent of environment, with Local Group and cluster galaxies coinciding in the various diagrams. As an example, due to the presence of a population of very low surface brightness dwarf spheroidal galaxies (dSphs) in the Fornax cluster, which may be tidally heated dwarf galaxies, the Fornax dwarf spheroidal galaxy (dSph) population is on average only 0.2 mag arcsec^{-2} fainter than the Local Group dSph populations. This offset is much too small to destroy the global relation between luminosity and central surface brightness.

We show that at $M_V \sim -14$ mag, the slopes of the photometric scaling relations involving the Sérsic parameters change significantly. This contradicts previous claims that the relations involving Sérsic parameters are pure power laws for all early-type galaxies and are, therefore, more fundamental than other photometric scaling relations derived from them. We argue that these changes in slope reflect the different physical processes that dominate the evolution of early-type galaxies in different mass regimes. As such, these scaling relations contain a wealth of information that can be used to test models for the formation of early-type galaxies.

Key words: galaxies: clusters: general – galaxies: dwarf – galaxies: fundamental parameters – galaxies: structure.

1 INTRODUCTION

Dwarf spheroidal galaxies (dSphs) are faint stellar systems ($M_V \gtrsim -14$ mag) with smooth elliptical isophotes. They are presumed to be the faint analogues of dwarf elliptical galaxies (dEs), which are usually defined as lying in the luminosity range $-19\,\mathrm{mag} \lesssim M_V \lesssim -14\,\mathrm{mag}$. Being found typically not more than a few hundred kiloparsecs away from a massive galaxy or in groups and clusters of galaxies, they show a strong predilection for high-density environments (Mateo 1998; Grebel, Gallagher & Harbeck 2003). Their dynamical mass-to-light ratios, derived by fitting dynamical models to their stellar velocity dispersion profiles or based on stability arguments, vary from a few tens up to a few hundreds, in solar units (Mateo 1998; Łokas 2002; Kleyna et al. 2005; De Rijcke et al. 2006; Lewis et al. 2007; Mateo, Olszewski & Walker 2008; Penny et al. 2008). This high mass-to-light ratio suggests the presence of copious amounts of dark matter that helps protect the embedded stellar

⋆E-mail: sven.derijcke@UGent.be

body of the dSph against the tidal forces of the massive host galaxy or of the galaxy cluster or group in which the dSph resides. This would explain why only a handful of dSphs in the Local Group show clear signs of an ongoing interaction, despite being close satellites of either the Milky Way or M31 (Johnston, Spergel & Hernquist 1995; Mateo et al. 1996; McConnachie & Irwin 2006; Lewis et al. 2007; Ségall et al. 2007). Many dSphs and dEs still contain an interstellar medium and some even host low-level star formation (Blitz & Robishaw 2000; Conselice et al. 2003b; De Rijcke et al. 2003; Grebel et al. 2003; Buyle et al. 2005; Lisker et al. 2006; Young et al. 2007), showing that the supernova explosions are not very efficient at expelling gas (Marcolini, Brighenti & D'Ercole 2003; Valcke, De Rijcke & Dejonghe 2008).

Bright elliptical galaxies, or Es, and dEs follow the same photometric and kinematic scaling relations (Graham & Guzmán 2003, hereafter GG03; Matković & Guzmán 2005; De Rijcke et al. 2005, hereafter D05; Smith Castelli et al. 2008). In the luminosity interval -24 mag $\lesssim M_V \lesssim -14$ mag, the parameters of the Sérsic profile follow simple power laws as a function of luminosity and early- and late-type galaxies trace parallel Tully–Fisher relations (De Rijcke et al. 2007). From this wealth of data, a picture of (dwarf) galaxy formation emerges that suggests an underlying unity in the physics driving the formation and evolution of stellar systems, with the environment playing a role that is in many situations subordinate to that of internal processes. More specifically, numerical simulations and semianalytic models of galaxy formation within a Λ cold dark matter (CDM) cosmology can account for the observed scaling relations when taking into account supernova feedback in galactic gravitational potential wells steepening with galaxy mass (Carraro et al. 2001; Nagashima & Yoshii 2004; Ricotti & Gnedin 2005; Marcolini et al. 2006; Valcke et al. 2008).

The goal of this paper is to investigate whether the photometric scaling relations traced by dEs and Es persist down to dSphs ($M_V \gtrsim -14$ mag). We also check for possible environmental influences other than the obvious density–morphology relation (i.e. the fact that the dEs/dSphs are found predominantly in high-density environments). We present new data based on our *Hubble Space Telescope* (*HST*)/Advanced Camera for Survey (ACS) imaging of dSphs/dEs in the Perseus cluster and combine these with data of early-type galaxies in the Antlia, Fornax and Virgo clusters and the Local Group (see Section 2). The resulting photometric scaling laws are presented in Section 3. We discuss the results in Section 4.

2 PHOTOMETRIC DATA

2.1 Perseus cluster data

The Perseus cluster (Abell 426) is one of the richest nearby galaxy clusters, with a redshift $v = 5366\,\mathrm{km\,s^{-1}}$ (Struble & Rood 1999) and a distance $D = 72$ Mpc [as given by NASA/IPAC Extragalactic Data base (NED)]. Due to its low Galactic latitude ($b \approx -13^\circ$), it has not been studied in as much detail as other nearby clusters, such as Fornax, Virgo and Coma. We have obtained high-resolution (*HST*) ACS Wide Field Camera (WFC) imaging in the F555W and F814W bands of five fields in the Perseus cluster core, in the immediate vicinity of NGC 1275 and NGC 1272, the cluster's brightest members, obtained in 2005 (program GO 10201). The scale of the images is 0.05 arcsec pixel^{-1}, with a field of view of 202×202 arcsec^2, providing a total survey area of $\sim$57 arcmin^2. The positions on the sky of these five pointings are presented in Fig. 1. Exposure times were 2368 and 2260 s for the F555W and F814W bands, respectively. The fields were chosen to cover the most likely cluster dSphs and dEs identified from ground-based imagery by Conselice, Gallagher & Wyse (2003a). For some of these, there is spectroscopic confirmation of their cluster membership (Penny & Conselice 2008). For the others, we use morphological criteria to decide cluster membership. The Concentration, Asymmetry, Smoothness (CAS) system for quantifying compactness, asymmetry and clumpiness/smoothness (Conselice et al. 2003b) proves very useful to reject, e.g., background spiral galaxies based on a smoothness criterion and background bright ellipticals based on a compactness criterion (see Penny et al. 2008). The Perseus data set straddles the dE-dSph transition at $M_V \sim -14$ mag and is, therefore, essential to the discussion that follows.

A detailed account of our photometric analysis of the *HST*/ACS images of Perseus dSphs and of the properties of the individual galaxies will be reported elsewhere (Penny et al., in preparation).

2.2 Data from the literature

The photometric data, including resolved photometry for surface brightness profiles, of the Local Group dSphs that are identified as Milky Way satellites are collected from Grebel et al. (2003) and Irwin & Hatzidimitriou (1995), adopting the distances listed in Grebel et al. (2003). Data of the M31 dSph satellites are taken from Peletier (1993), Caldwell (1999), Grebel et al. (2003), McConnachie & Irwin (2006), McConnachie, Arimoto & Irwin (2007) and Zucker et al. (2007). Data of three Local Group dSphs that are not linked to a giant host galaxy, the Tucana dSph, DDO210 and KKR25, come from Saviane, Held & Piotto (1996), Grebel et al. (2003) and McConnachie & Irwin (2006). D05 and Mieske, Hilker & Infante (2007) provide photometric data on the early-type dwarf galaxy population of the Fornax cluster. Half of the D05 sample consists of dEs from the NGC 5044 and NGC 5989 groups. The data of the dSphs and dEs in the Antlia cluster are taken from Smith Castelli et al. (2008). Data for the giant elliptical and for Coma dEs are taken from GG03.

This sample of early-type galaxies comprises dwarf spheroidals, with $-14\,\mathrm{mag} \lesssim M_V \lesssim -8$ mag, dwarf ellipticals, with $-19\,\mathrm{mag} \lesssim M_V \lesssim -14$ mag, and bright ellipticals, with $M_V \lesssim -19$ mag. We plot the positions of the sample galaxies in diagrams of V-band absolute magnitude versus (i) half-light radius R_e (in kpc), versus (ii) the Sérsic exponent n of the best-fitting Sérsic profile, versus (iii) the central V-band surface brightness of the best-fitting Sérsic profile, and versus (iv) $V - I$ colour. These diagrams are shown in Fig. 2. The data sets are plotted using different symbols that are explained within each panel of the figure. The presence of a data set in a given panel depends solely on the availability of the required data.

3 PHOTOMETRIC SCALING RELATIONS

3.1 Method

For our Perseus dSphs/dEs, we measure the profiles of surface brightness, position angle and ellipticity as a function of the geometric mean of major and minor axis distance, denoted by a and b, respectively, using our own software. Basically, the code fits an ellipse through a set of positions where a given surface brightness level is reached. Residual cosmics, background galaxies and foreground stars are masked and not used in the fit. The shape of an isophote, relative to the best-fitting ellipse, is quantified by expanding the surface brightness variation along this ellipse in a fourth-order Fourier

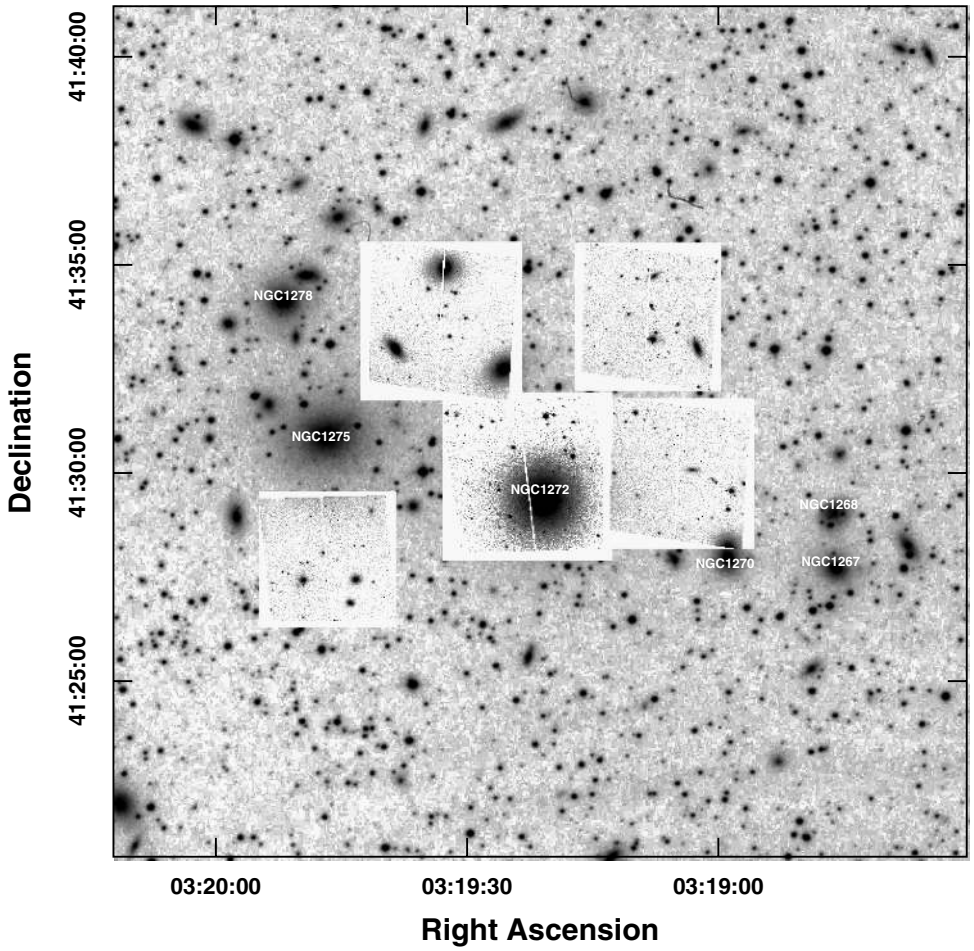

Figure 1. Position on the sky of our five *HST*/ACS pointings near the core of the Perseus cluster. The *HST*/ACS fields are overplotted on to a DSS image of the cluster. The NGC numbers of the most prominent cluster members are indicated in the figure.

series with coefficients S_4, S_3, C_4 and C_3:

$$I(a,\theta) = I(a)\,[1 + C_3(a)\cos(3\theta) + C_4(a)\cos(4\theta) + S_3(a)\sin(3\theta) + S_4(a)\sin(4\theta)]\,. \quad (1)$$

Here, $I(a)$ is the mean surface brightness of an isophote with semimajor axis a, and the angle θ is measured from the major axis. Apparent ABMAG magnitudes in the F555W and F814W bands are calculated using the zero points given by Sirianni et al. (2005). These magnitudes are corrected for interstellar reddening adopting the colour excess $E(B-V) = 0.171$ mag (Schlegel, Finkbeiner & Davis 1998) and using the prescriptions given in Sirianni et al. (2005). These reddening-corrected magnitudes are finally converted into Johnson V- and I-band magnitudes using the transformations of Sirianni et al. (2005).

The smooth representation of a galaxy's surface-brightness profile, $I(a, \theta)$, is then subtracted from the original image. We have checked that the result is indeed a pure noise image, free of residuals. $I(a, \theta)$ is integrated over circular apertures out to the last isophote we could reliably measure (which is at $\mu_{\rm ABMAG} \approx 27$ mag arcsec^{-2} in both the F555W and F814W images) to derive model-independent structural parameters, such as the total apparent magnitude and the half-light radius in each band. For such deep images of galaxies with a roughly exponentially declining surface brightness profile, this truncation results in an insignificant uncertainty on the total luminosity, of the order of a few per cent (see also D05). $V-I$ colours are measured using the V- and I-band flux inside the I-band half-light radius. We fit a Sérsic profile, given by

$$\mu_V(r_p) = \mu_{0,V} + 1.0857\left(\frac{r_p}{r_0}\right)^{1/n}, \quad (2)$$

to the V-band surface brightness profiles of the program galaxies, expressed in mag arcsec^{-2}. Here, the equivalent radius $r_p = \sqrt{ab}$ is the geometric mean of the isophotes' semimajor axes a and semiminor axes b, $\mu_{0,V}$ is the central V-band surface brightness, in mag arcsec^{-2}, r_0 is a scale-length, in arcseconds, and the exponent n is a shape parameter with $n = 1$ giving an exponentially declining profile and $n = 4$ corresponding to the de Vaucouleurs-profile typical of giant ellipticals.

For the Antlia cluster, we adopt a distance of 35.1 Mpc, as advocated by Smith Castelli et al. (2008). This distance estimate is based on surface-brightness fluctuation (SBF) distances to two giant Es in this cluster. As in D05, we place the Fornax cluster at a distance of 19.7 Mpc, the NGC 5044 group at 35.1 Mpc, the NGC 5898 group at 30.3 Mpc, and the NGC 3258 group at 40.7 Mpc, all in good agreement with SBF distances (Tonry et al. 2001; Jerjen 2003). For the GG03 data set, only B-band photometry is available. We convert B-band magnitudes into V-band magnitudes using a $B-V$ colour–magnitude relation (CMR) constructed from the $M_V - (V-I)-$[Fe/H] relation (see Section 3.5) in combination with SSP models for 10-Gyr-old stellar populations (Vazdekis et al.

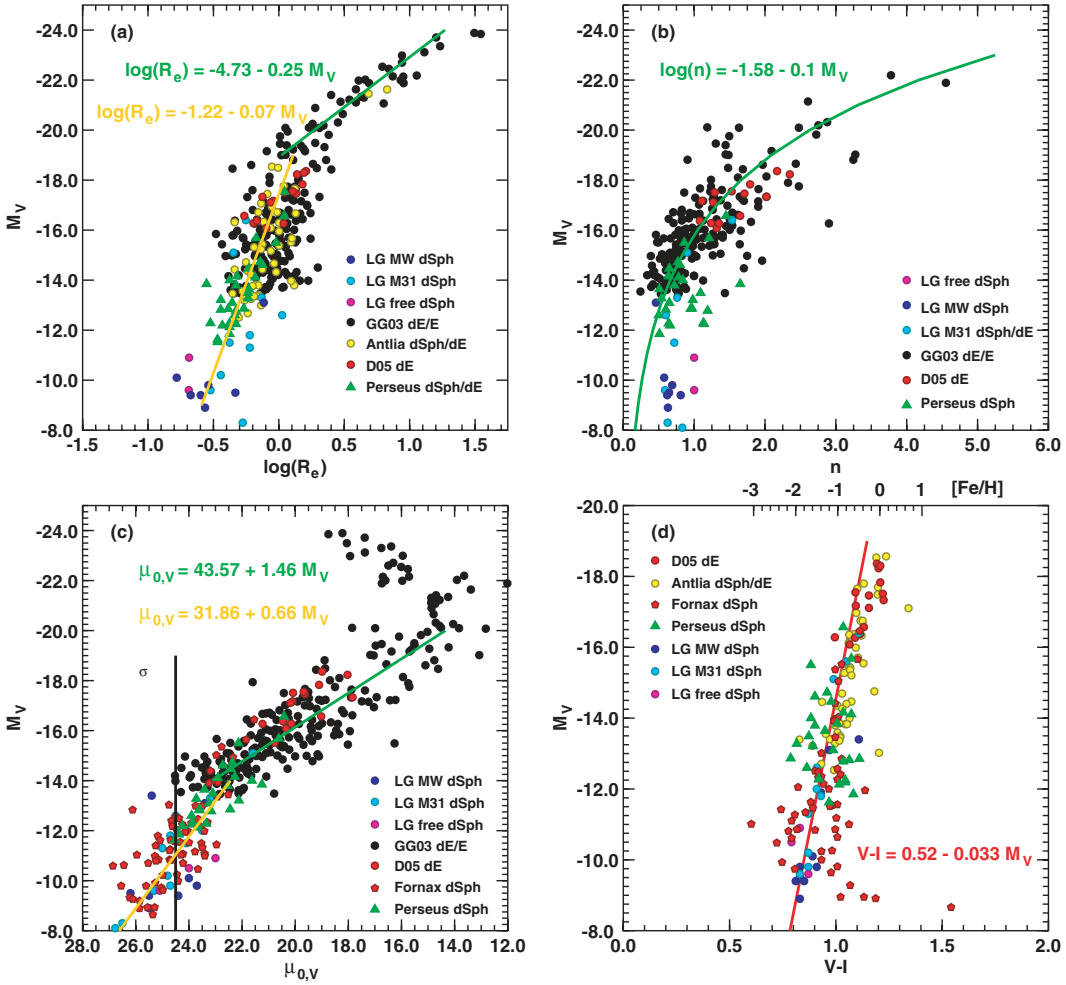

Figure 2. Photometric scaling relations of dwarf spheroidal, dwarf elliptical and elliptical galaxies. (a) Half-light radius, R_e (kpc), versus absolute V-band magnitude, M_V. The green line traces the relation $\log(R_e) = -4.73 - 0.25 \times M_V$ of the bright ellipticals, whereas the orange line indicates the relation $\log(R_e) = -1.22 - 0.07 \times M_V$ of the dEs and dSpshs. (b) The Sérsic parameter n versus absolute V-band magnitude. The green curve traces the $\log(n) \propto 0.1 \times M_V$ relation of GG03. (c) Central surface brightness $\mu_{0,V}$ (mag arcsec^{-2}), derived by fitting a Sérsic law to the observed galaxies' surface brightness profiles, versus absolute V-band magnitude. The green curve traces the relation $\mu_{0,V} \propto 1.46 \times M_V$ of the dwarf and giant ellipticals; the orange curve is the $\mu_{0,V} \propto 0.66 \times M_V$ relation of the dwarf spheroidals. (d) $V - I$ colour versus absolute V-band magnitude (the top x-axis is labelled in metallicity, quantified by [Fe/H], using an empirical relation between $V - I$ and [Fe/H] (Couture et al. 1990; Kundu & Whitmore 1998). The red line traces the linear fit to the Fornax cluster M_V versus $V - I$ relation by Mieske et al. (2007). The photometric data of the Local Group dSphs (LG MW dSph for the Milky Way satellites; LG M31 dSph/dE for the M31 satellites; LG free dSph for the dSphs that are not linked to a giant host galaxy) come from Peletier (1993), Irwin & Hatzidimitriou (1995), Saviane et al. (1996), Caldwell (1999), Grebel et al. (2003), McConnachie & Irwin (2006), McConnachie et al. (2007) and Zucker et al. (2007). The other data sets are from GG03 (GG03 dE/E), D05 (D05 dE), Mieske et al. (2007) (Fornax dSph), Smith Castelli et al. (2008) (Antlia dSph/dE) and this work (Perseus dSph).

1996). This relation interpolates between $B - V \approx 0.7$ mag at $M_B = -8$ mag and $B - V \approx 1.0$ mag at $M_B = -22$ mag. As we show below, our conclusions do not depend on this slight colour correction applied to the GG03 data set. There are no systematic deviations of the colour-corrected GG03 data set with respect to other data sets with which it overlaps in luminosity. Applying a constant mean colour correction $\langle B - V \rangle = 0.8$ mag (van Zee, Barton & Skillman 2004) yields essentially the same results.

For the Local Group dSphs for which no Sérsic parameters can be found in the literature, we fit Sérsic profiles, with an added constant background density of stars, to the star counts of the dSphs presented in Irwin & Hatzidimitriou (1995).

We now place these early-type galaxies in diagrams correlating the V-band absolute magnitude M_V, the Sérsic exponent n, the extrapolated central surface brightness $\mu_{0,V}$ and the $V - I$ colour. The goal is to investigate the behaviour of the relations between these structural parameters as a function of luminosity in the range -24 mag $< M_V < -8$ mag and of environment, using galaxies from the Local Group, the NGC 5044 and NGC 5898 groups, and the Antlia, Fornax, Perseus and Coma clusters.

3.2 Luminosity versus half-light radius

We plot V-band absolute magnitude against half-light radius, denoted by R_e, in Fig. 2(a). Es and gEs follow a trend of increasing half-light radius with increasing luminosity, which can be quantified as

$$\log(R_e) = (-4.73 \pm 0.47) - (0.25 \pm 0.02) \times M_V \quad (3)$$

between $M_V \sim -19$ and ~ -24 mag (green line in Fig. 2a). In the range $-19\,\mathrm{mag} \lesssim M_V \lesssim -14$ mag, on the other hand, the half-light radius of dEs increases much more slowly as a function of luminosity, with

$$\log(R_\mathrm{e}) = (0.92 \pm 0.14) - (0.05 \pm 0.01) \times M_V \quad (4)$$

(see also GG03; D05; Graham & Worley 2008; Smith Castelli et al. 2008). In the very low luminosity dSph regime, radius again appears to increase slightly more rapidly with luminosity as

$$\log(R_\mathrm{e}) = (-1.40 \pm 0.16) - (0.09 \pm 0.01) \times M_V, \quad (5)$$

between $M_V \sim -8$ and ~ -14 mag. This trend appears to continue for even fainter Milky Way satellites (Martin, de Jong & Rix 2008). The very gentle slope change around $M_V \sim -14$ mag seems to be caused mostly by the GG03 data set. All other data sets rather suggest that half-light radius behaves as a power law as a function of luminosity in the regime $M_V \gtrsim -19$ mag. A fit to the data of the dwarf galaxies fainter than $M_V = -19$ mag from the D05, Antlia, Perseus and Local Group data sets gives

$$\log(R_\mathrm{e}) = (-1.22 \pm 0.11) - (0.07 \pm 0.01) \times M_V \quad (6)$$

(orange line in Fig. 2a). The gentle curvature of the $M_V - R_\mathrm{e}$ relation around $M_V \sim -19$ mag was shown by GG03 to be a consequence of the power-law dependence of the Sérsic parameters on galaxy luminosity.

One small caveat, however, the half-light radius can be measured in a number of different ways which do not necessarily yield the same result for a given galaxy. One can, for instance, use the geometric mean of the semimajor axis and semiminor axis of the elliptical isophote that encloses half the light as a measure for R_e. Or, one can fit a Sérsic law to the surface brightness profile, evaluated as a function of equivalent radius, and adopt the half-light radius of this model profile, as in GG03. Or one can construct the growth curve model independently by integrating the observed surface brightness over circular apertures and thus derive a half-light radius, as in D05. For spherically symmetric galaxies, these different approaches obviously yield the same result. For very flattened galaxies, they may differ. If the early-type galaxy population shows a trend of mean flattening with luminosity (see e.g. Bender et al. 1989), this might introduce a spurious trend of half-light radius with luminosity.

In order to check how large this systematic effect can be, we create synthetic galaxy images using flattened Sérsic profiles with different flattenings $\epsilon = 10(1 - b/a)$ and Sérsic exponents n. The half-light radius is then measured as the geometric mean of the semimajor axis and semiminor axis of the elliptical isophote that encloses half the light and by integrating over circular isophotes. The difference between the two approaches is plotted in Fig. 3 as a function of flattening ϵ and Sérsic n. The maximum deviation is obtained for small n and strong flattening, and is not larger than $\Delta\log(R_\mathrm{e}) \approx 0.15$. This is smaller than the scatter on the observed scaling relations. We, therefore, do not expect to see any significant systematic trend of half-light radius with flattening as a result of the particular way it was measured.

Although the data show considerable scatter, especially in the dwarf regime, it is striking that galaxies from a wide range of environments trace a continuous M_V versus R_e relation over a range of six orders of magnitude in luminosity.

3.3 Luminosity versus Sérsic *n*

It is well known that the early-type galaxies brighter than $M_V \sim -14$ mag trace a single M_V versus n relation. This relation is quantified as $\log(n) = -1.4 - 0.1 \times M_B$ by Jerjen & Binggeli (1997),

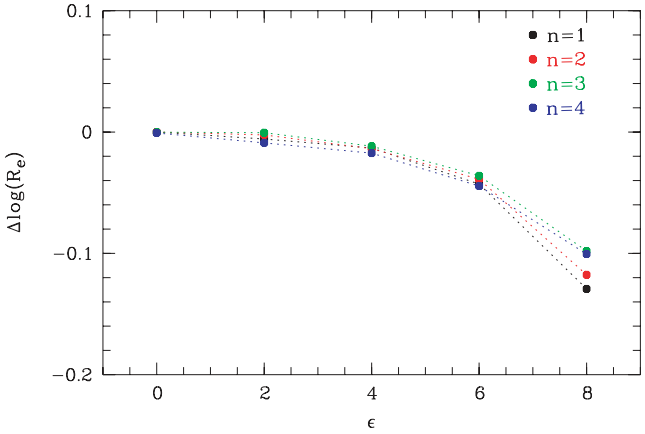

Figure 3. Deviation of the logarithm of the half-light radius measured using circular apertures from the half-light radius defined as the geometric mean of the semimajor axis a and semiminor axis b of the elliptical isophote that encloses half the light as a function of flattening $\epsilon = 10(1 - b/a)$. This exercise was performed for synthetic surface brightness profiles with Sérsic $n = 1$, 2, 3 and 4. The maximum deviation is not larger than $\Delta\log(R_\mathrm{e}) \approx 0.15$.

as $\log(n) = -1.88 - 0.12 \times M_{\mathrm{F606W}}$ by GG03, and as $\log(n) = -1.52 - 0.11 \times M_B$ by Graham & Worley (2008). These authors fit Sérsic profiles to the observed surface brightness profiles, evaluated as a function of equivalent radius. However, it is also possible to fit the growth curve, constructed by integrating a galaxy image over circular apertures, with the growth curve of the Sérsic profile. This approach is advocated by Prugniel & Simien (1997). The latter method of determining the Sérsic exponent n assigns a large weight to the outer data points, and has the obvious advantage of yielding a Sérsic model with the same total luminosity as the observed galaxy. However, the model's surface brightness profile does not necessarily provide an acceptable fit to that of the observed galaxy. The former method, on the other hand, assigns a large weight to the inner data points. This method has the benefits that clearly the non-Sérsic components (such as a nuclear star cluster of a stellar halo) can be omitted from the fit, and that the model provides a good fit to the observed surface brightness profile (at least within some specified radial range). It does not, however, necessarily provide a good approximation of the galaxy's growth curve.

As an example, we apply both methods to the Sculptor dSph, with star count data taken from Irwin & Hatzidimitriou (1995), and to our new *HST*/ACS photometry of CGW45, a Perseus cluster dE, taken from the sample of Conselice et al. (2003a). The observed surface brightness profile of CGW45, $\mu(r)$ is converted into a 'star counts' profile in arbitrary units, $n(r)$ using

$$n(r) = 10^{(20-\mu(r))/2.5}. \quad (7)$$

Sculptor is an example of a galaxy whose surface brightness profile deviates from the Sérsic law at large radii; CGW45, a nucleated dE, on the other hand, deviates from a Sérsic profile at small radii. The differences between the two methods for obtaining n are illustrated in Fig. 4. A fit to the stellar density profile of Sculptor yields $n \approx 0.7$; a fit to the growth curve results in $n \approx 1.0$. The former method yields a very good approximation to both the growth curve and the density profile within the inner 30 arcmin but fails at larger radii. The latter method gives a superior fit to the growth curve outside 30 arcmin but fails to provide an acceptable fit to the density profile.

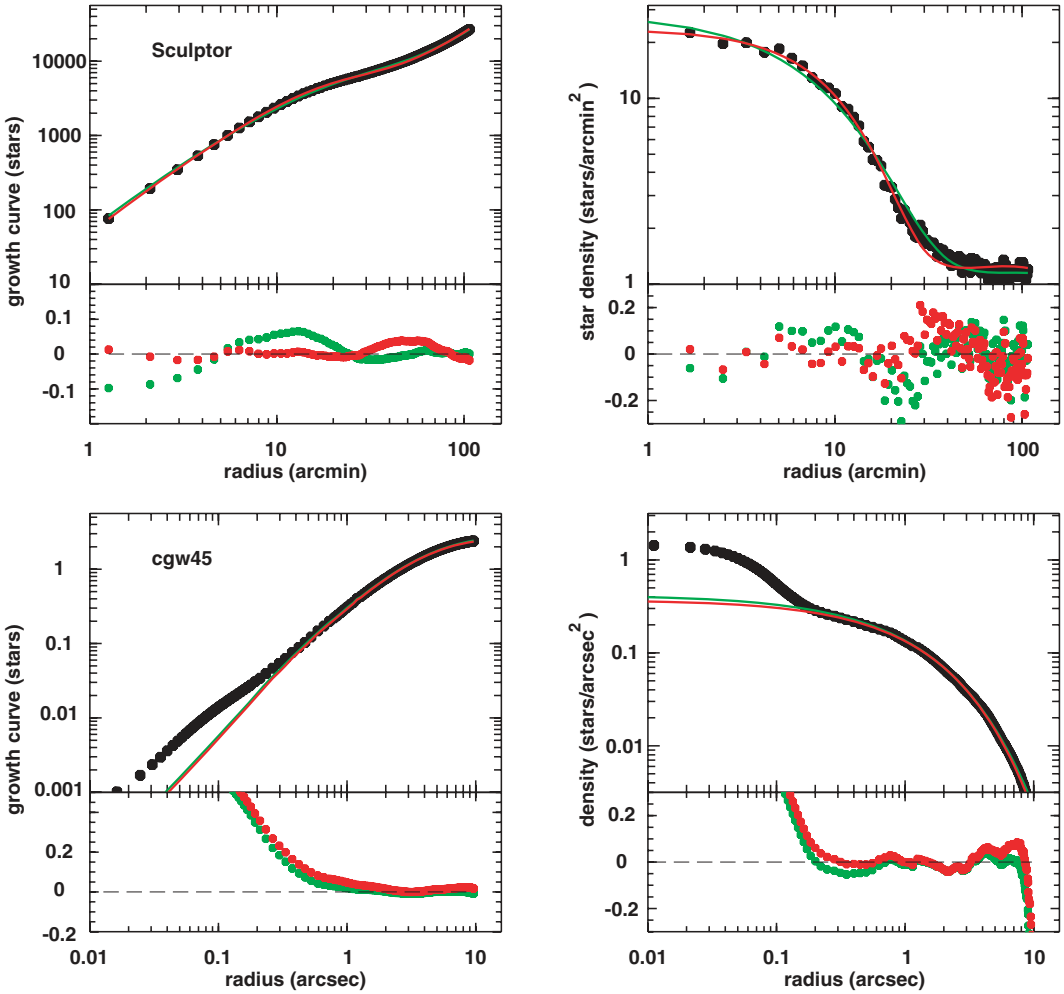

Figure 4. The growth curve (left-hand panels) and the radial profile of the projected stellar density (right-hand panels) of the Sculptor dSph (top row), taken from Irwin & Hatzidimitriou (1995), and the Perseus cluster dSph CGW45 (bottom row), taken from the Conselice et al. (2003a) sample. The stellar density of CGW45 is in arbitrary units. The black dots represent the data; the red line is a Sérsic profile fitted to the projected stellar density profile; the green line is a Sérsic profile fitted to the growth curve. Under each panel, the relative residuals are plotted in the same colours. Sculptor is an example of a galaxy whose surface brightness profile deviates from a Sérsic profile at large radii; CGW45 is a nucleated dwarf elliptical galaxy and deviates from a Sérsic profile at small radii.

In the case of CGW45, both methods give $n \approx 1.4$. The central nucleus prevents both methods from yielding a good fit to the growth curve within the inner 0.2 arcmin. Omitting the central 0.2 arcmin results in a very good Sérsic fit to the density profile.

Choosing between these two methods is clearly a matter of taste. Here, as in GG03, we wish n to reflect the shape of the surface brightness profile of the bulk of the galaxy and, therefore, opt to fit a Sérsic profile to the surface brightness profile evaluated as a function of equivalent radius.

It is obvious from Fig. 2(b) that for galaxies fainter than $M_V \sim -14$ mag, the relation between luminosity and n appears to break down. The dwarf spheroidals for which the Sérsic exponent n is available, i.e. the Local Group dSphs, for some of which we have measured n using published star counts (Irwin & Hatzidimitriou 1995), and our new Perseus cluster dSphs, all lie in the range $n \approx 0.5$ to 1.0, essentially independent of galaxy luminosity. This n is significantly larger than that predicted by the scaling relations mentioned before (green curve). It is, therefore, clear that in the dSph regime, the power-law behaviour of the $M_V - n$ relation breaks down.

From Fig. 5, it is clear that a Sérsic profile with $0.5 \lesssim n \lesssim 1$ is almost indistinguishable from a King model with a concentration $c = r_{\rm tidal}/r_{\rm core}$ in the range 3 to 10, which is typical for dSphs. In this figure, we plot the radial profile of projected stellar density of the Sculptor dSph (black data points), taken from Irwin & Hatzidimitriou (1995), overplotted with the best-fitting Sérsic profile (red line) and the King profile (green line). The Sérsic profile has a shape parameter $n = 0.7$; the concentration of the King profile is $c = r_{\rm tidal}/r_{\rm core} = 4.25$. Both three-parameter laws give a very good representation of the data, taking into account a background density of 1.13 arcmin^{-2}. Thus, the breakdown of the power-law dependence of n on luminosity in the dSph regime might have been foreseen based on the already known fact that $c \gtrsim 3$ for dSphs.

Sharina et al. (2008) fit the surface brightness profiles of a sample of Local Volume dSphs, dIrrs and brighter late-type galaxies with exponentials and investigate the resulting relation between luminosity and exponential scale-length, denoted by h. They note that the luminosity–h relation becomes almost flat in the dSph regime. This is a direct consequence of the $M_V - R_{\rm e}$ and $M_V - n$ relations presented here. We generate synthetic Sérsic surface brightness profiles

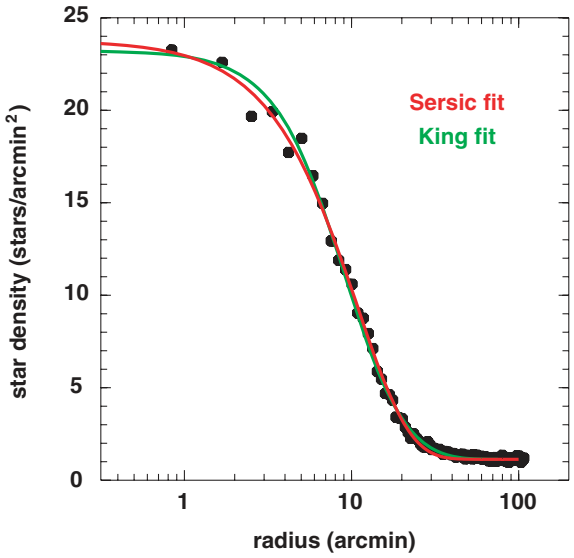

Figure 5. The radial profile of the projected stellar density overplotted (black dots) with the best-fitting Sérsic profile (red line) and theKing profile (green line). The Sérsic profile has a shape parameter $n = 0.7$; the concentration of the King profile is $c = r_{\rm tidal}/r_{\rm core} = 4.25$. A constant background of 1.13 arcmin^{-2} was added to the two profiles.

using the latter relations. We fit these synthetic surface brightness profiles with exponentials and thus constructed a $M_V - h$ relation. This relation is in excellent agreement with the one found observationally by Sharina et al. (2008). Between $M_V = -10$ and -14 mag, the exponential scale-length increases only from 0.25 to 0.5 kpc. This $M_V - h$ relation is much shallower than the $M_V - R_{\rm e}$ relation because of the increase of n with M_V, which makes brighter galaxies more centrally concentrated than fainter ones.

3.4 Luminosity versus central surface brightness

The $M_V - \mu_{0,V}$ diagram is presented in Fig. 2(c). The vertical black line marks the 1σ background noise level of our *HST*/ACS images, translated into a V-band surface brightness. We can only derive reliable surface photometry for galaxies with a central surface brightness above roughly this background limit, corresponding to $\mu_{{\rm BG},v} = 24.5$ mag arcsec^{-2}. For galaxies brighter than $M_V \sim -14$ mag, the central surface brightness, estimated by extrapolating the best-fitting Sérsic profile to zero radius, varies as a power of the luminosity. Only the very brightest cored gEs deviate from this power law. This underlying unity between Es and dEs was not initially appreciated since it is not reflected in the luminosity versus mean and effective surface brightness diagrams GG03. Using the Sérsic parameters as fundamental morphological parameters, the assumed structural dichotomy between Es and dEs has disappeared and the idea that similar physical processes have governed the evolution of *all* spheroidal galaxies was put forward.

However, for galaxies fainter than $M_V \sim -14$ mag, the slope of the $\mu_{0,V} - M_V$ relation changes significantly. This is a direct consequence of the near constancy of n in this luminosity regime, with $n \approx 0.8$ (Fig. 2b), and the observed $M_V - R_{\rm e}$ relation (Fig. 2a). At constant n, the latter translates into a $M_V - r_0$ relation, with r_0 the scale-radius of the Sérsic profile, that is completely similar to the $M_V - R_{\rm e}$ relation. Given $n = 0.8$ and this $M_V - r_0$ relation, the central surface brightness should follow the relation

$$\mu_{0,V} = 29.68 + 0.46 \times M_V \qquad [\rm dSph]. \tag{8}$$

A linear fit to the dSphs from the Local Group, the Perseus cluster and the Fornax cluster yields

$$\mu_{0,V} = (31.86 \pm 0.43) + (0.66 \pm 0.04) \times M_V \qquad [\rm dSph], \tag{9}$$

plotted as an orange line in Fig. 2. This differs signifcantly from the relation

$$\mu_{0,V} = (43.57 \pm 0.96) + (1.46 \pm 0.06) \times M_V \qquad [\rm dE + E] \tag{10}$$

fitted to the GG03 dEs and Es (green line). It is important to note that the slope change around $M_V = -14$ mag is immediately evident from the data sets for the dwarf populations of the Fornax cluster and the Perseus cluster, which cover the transition region in the $M_V - \mu_{0,V}$ diagram. Hence, within the same environment, dSphs ($M_V \gtrsim -14$ mag) and dEs/Es ($M_V \lesssim -14$ mag) follow a $M_V - \mu_{0,V}$ relation with a slope that varies as a function of luminosity. Early-type galaxies from different environments (the Local Group, Fornax, Coma, Perseus, ...) all fall on the same $M_V - \mu_{0,V}$ relation. This shows that the slope of this relation is a strong function of galaxy luminosity but not of environment.

As Mieske et al. (2007) note, their sample includes a population of dSphs that have much fainter central surface brightnesses than those of the Local Group. Our *HST*/ACS imaging, unfortunately, does not go deep enough to detect such a population in the Perseus cluster. In order to quantify the effect of this population on the global scaling relation, we measure the surface brightness deviation of the Fornax dSphs and of the Local Group and Perseus cluster dSphs from the straight-line relation given by equation (9). This deviation of surface brightness from the mean relation is denoted by $\Delta\mu_{0,V}$. Only galaxies fainter than $M_V = -14$ mag have been selected for this exercise. For the Fornax dSphs, the distribution of this deviation shows a pronounced tail towards large, positive $\Delta\mu_{0,V}$ (see Fig. 6).

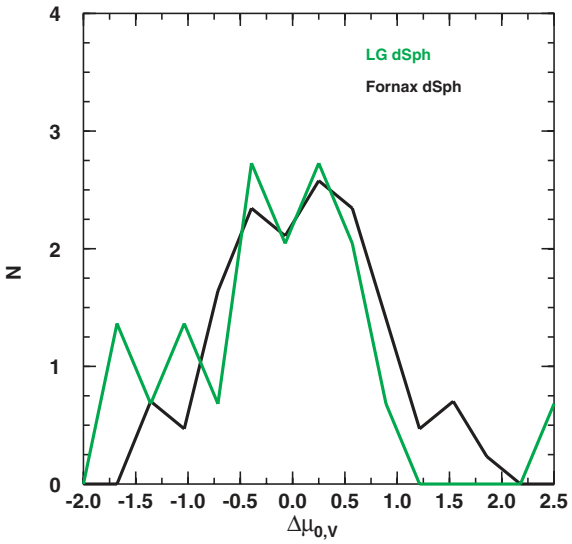

Figure 6. Distribution of the surface brightness deviation of the Local Group dSphs (green curve) and Fornax dSphs (black curve) from the mean relation $\mu_{0,V} = (31.86 \pm 0.43) + (0.66 \pm 0.04) \times M_V$, denoted by $\Delta\mu_{0,V}$. Both distributions have the same normalization. Only galaxies fainter than $M_V = -14$ mag have been selected for this exercise. The Fornax cluster clearly contains a low-surface brightness population that is absent from the other data sets. The offset between the means of these distributions is about 0.2 mag arcsec^{-2}.

This is the signature of the low-surface-brightness population. This population is clearly absent from the Local Group and Perseus dSph data sets. However, the mean $\Delta\mu_{0,V}$ of the Fornax dSph population differs less than 0.2 mag arcsec^{-2} from that of the Perseus and Local Group populations.

Interestingly, dSphs seem to trace the same $M_V - \mu_{0,V}$ relation as the dIrrs within the local 10 Mpc volume, which was quantified as

$$\mu_{0,V} = 29.29 + 0.52 \times M_V \qquad \text{[dIrr]} \tag{11}$$

by Sharina et al. (2008). If star formation was somehow switched off in dIrrs that are initially on this relation, fading of M_V and $\mu_{0,V}$ over time by roughly the same amount (in magnitudes) would result in exactly such a population of very low surface brightness dSph-like objects. So, while Es and dEs seem to follow a linear relation between M_V and $\mu_{0,V}$, dSphs deviate significantly from this relation. They have a higher central surface brightness than predicted by the extrapolated relation of dEs and Es, albeit with the existence of a possible cluster population of very low surface brightness dSphs, which, Mieske et al. (2007) surmise could be a population of tidally heated dwarf galaxies.

3.5 Luminosity versus $V - I$ colour

The $V - I$ colours of early-type dwarfs of the Perseus cluster, with both V- and I-band magnitudes measured within the I-band half-light radius, are plotted versus V-band absolute magnitude in Fig. 2(d). The same data for the Fornax cluster early-type dwarfs have been taken from Mieske et al. (2007) and plotted in the same panel. A linear fit to the Fornax cluster M_V versus $V - I$ relation is overplotted (full red line). The Perseus dwarfs obviously adhere quite closely to the CMR defined by the Fornax dwarfs.

In order to investigate the physical nature of the CMR, we convert the iron abundance [Fe/H], measured by Michielsen et al. (2007) for the D05 sample of cluster and group dEs, into a $V - I$ colour using an empirical colour–metallicity relation calibrated for old stellar populations, such as globular clusters (Couture, Harris & Allwright 1990; Kundu & Whitmore 1998). This places the D05 dwarfs essentially along the extension of the Mieske et al. (2007) CMR. The same exercise can be done for the Local Group dSphs, with the metallicity taken from the compilation by Grebel et al. (2003), with the same result: they end up following the Mieske et al. (2007) CMR. This already suggests that the $V - I$ CMR of early-type dwarf galaxies is, in fact, a luminosity–metallicity relation. As a further test, we convert the $C - T_1$ colours of the Antlia dSphs/dEs, measured by Smith Castelli et al. (2008), into $V - I$ colours using empirical $(C - T_1)-$[Fe/H] and [Fe/H]$-(V - I)$ relations as an intermediate step. This places the Antlia dSphs/dEs almost exactly on the extension of the CMR of the Fornax dSphs.

Thus, it appears that the observed $V - I$ CMR of early-type galaxies, from dwarfs to giants, is a luminosity–metallicity relation of galaxies that have stopped forming stars sufficiently long ago for there being almost no age information left (see also Smith Castelli et al. 2008, and references therein).

4 DISCUSSION AND CONCLUSIONS

We have collected photometric data of dSphs/dEs from different galaxy groups and clusters. Analogous to Goto et al. (2003), we quantify the galaxy densities of the different environments we are studying as the projected density of galaxies brighter than $M_B = -19$ mag within the radius d_5 that contains five such galaxies,

Table 1. Central bright-galaxy density, measured by $\log(\Sigma_5)$ (see equation 12), of the different environments from which the data set was composed.

Group/cluster	$\log(\Sigma_5)$
Local Group	−0.9
NGC 5898 group	−0.7
Fornax cluster	0.5
NGC 5044 group	0.7
Antlia cluster	1.5
Perseus cluster	1.8
Coma cluster	2.0

or

$$\Sigma_5 = \frac{5}{\pi d_5^2}\ \text{galaxies}\,\text{Mpc}^{-2}. \tag{12}$$

The $\log(\Sigma_5)$-values of the different environments from which we compiled the data set are listed in Table 1.

The Local Group and the NGC 5989 group constitute the sparsest environments covered by the data set [the NGC 5989 group consists of two bright ellipticals, NGC 5903 and NGC 5898, and a few tens of much fainter galaxies; Gourgoulhon, Chamaraux & Fouqué (1992) list only three group members brighter than $M_B \approx -18$ mag]. The Fornax cluster and the NGC 5044 group have comparable, intermediate bright galaxy densities. The Coma, Perseus and Antlia clusters have the most extreme central bright galaxy densities. Obviously, the data set contains early-type galaxies from a wide variety of environments.

There is considerable uniformity in the photometric properties of early-type galaxies, from dwarfs to giants. Photometric parameters quantifying the structure and stellar populations of early-type galaxies, such as the half-light radius, R_e, the central surface brightness $\mu_{0,V}$, the Sérsic exponent n and $V - I$ colour all correlate with galaxy luminosity over a range of more than six orders of magnitude in luminosity. Misgeld, Mieske & Hilker (2008) found the same result based on observations of the dwarf population of the Hyda I cluster. The scaling relations involving the Sérsic parameters, contrary to previous claims, do not keep a constant slope over the whole luminosity range. The Sérsic exponent n varies with luminosity L as $n \propto L^{0.25-0.3}$ for galaxies brighter than $M_V \approx -14$ mag but scatters around a constant value within the range $n \approx 0.5$–1.0 for fainter dSphs. This is in agreement with the fact that the surface brightness profiles of dSphs can be well approximated by King profiles with a concentration in the range $c \approx 3$–10. Central surface brightness increases with luminosity until the formation of the very brightest, cored ellipticals. The cores in the most luminous ellipticals are thought to result from the partial evacuation of the nuclear region by coalescing black holes (see GG03 and references therein). At $M_V \approx -14$ mag, the slope of the $M_V - \mu_{0,V}$ changes abruptly. We have shown that the M_V versus $V - I$ is essentially a metallicity–luminosity relation of old stellar populations, keeping the same slope over the whole luminosity range investigated here.

Clearly, the absolute magnitude $M_V \approx -14$ mag is not just an arbitrary divide between dSphs and dEs. The rather abrupt changes in the slopes of some of the photometric scaling relations suggest that below and above this luminosity, different physical processes dominate the evolution of early-type galaxies. The near-independence of these scaling relations with respect to environment and the physical differences between dSphs and dEs will be investigated theoretically using N-body/SPH-models in another paper in this series (De Rijcke

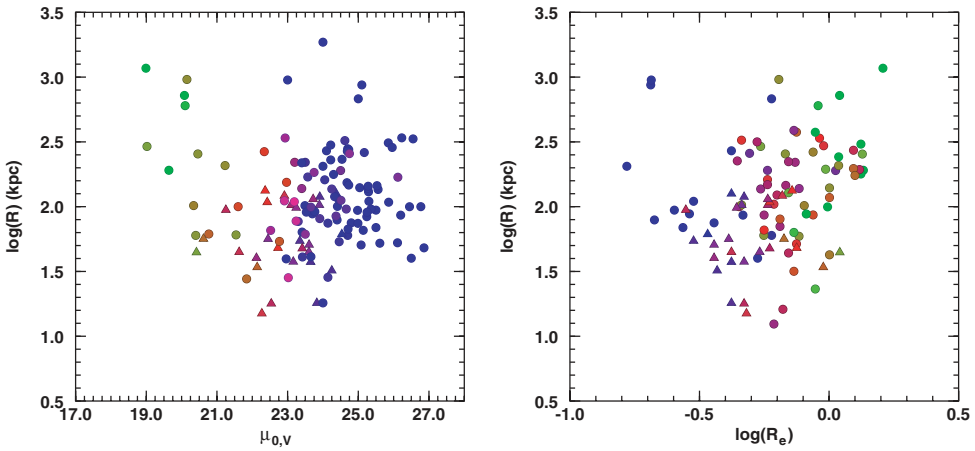

Figure 7. Central surface brightness, $\mu_{0,V}$ (left-hand panel), and half-light radius, R_e (right-hand panel), as a function of projected distance (in kpc), R, to the nearest bright galaxy (with $M_V < -20$ mag). The triangle data points are the Perseus dSphs. In the left-hand panel, the necessary data are available for the dSphs/dEs of the Local Group, the Perseus dSphs and the Fornax cluster dSphs/dEs from D05 and Mieske et al. (2007). In the right-hand panel, we use data from the dSphs/dEs of the Local Group, the Perseus dSphs, the Fornax cluster dEs from D05 and the Antlia dSpsh/dEs from Smith Castelli et al. (2008). The data points are colour coded according to their absolute luminosity, from blue ($M_V = -11$ mag) over red ($M_V = -14$ mag) to green ($M_V = -18$ mag). While there is no statistically significant correlation between these structural parameters and distance to the nearest bright galaxy there is a clear correlation with luminosity.

et al., in preparation). In a sense, the divide between dEs and Es, which has historically been placed at $M_V \approx -19$ mag, seems more arbitrary since the behaviour of the basic parameters describing the shapes of the surface brightness profiles as a function of luminosity (i.e. the Sérsic parameters) does not change. A comparison of numerical simulations with observed scaling relations suggests that the luminosity dependence of the Sérsic parameters is due to the fact that the effects of supernova feedback become more important as galactic gravitational potential wells become more shallow for lower galaxy masses (Carraro et al. 2001; Nagashima & Yoshii 2004; Valcke et al. 2008). This causes dEs to be more diffuse and to have stars orbiting with lower velocities than predicted by the extrapolated relations for Es (Held et al. 1992; GG03; Matković & Guzmán 2005; D05).

These scaling relations are amazingly insensitive to (local) environment. In Fig. 7, we show the central surface brightness, $\mu_{0,V}$ (left-hand panel), and half-light radius, R_e (right-hand panel), as a function of projected distance (in kpc), R, to the nearest bright galaxy (with $M_V < -20$ mag). The triangle data points are the Perseus dSphs. In the left-hand panel, the necessary data are available for the dSphs/dEs of the Local Group, the Perseus dSphs and the Fornax cluster dSphs/dEs from D05 and Mieske et al. (2007). In the right-hand panel, we use data from the dSphs/dEs of the Local Group, the Perseus dSphs, the Fornax cluster dEs from D05 and the Antlia dSpsh/dEs from Smith Castelli et al. (2008). The data points are colour coded according to their absolute luminosity, from blue ($M_V = -11$ mag) over red ($M_V = -14$ mag) to green ($M_V = -18$ mag). While there is no statistically significant correlation between these structural parameters and distance to the nearest bright galaxy, there is a strong correlation with luminosity.

We have also plotted these quantities as a function of distance to the cluster or group centre divided by the virial radius R_{200}. Again, no correlation with position becomes apparent. The galaxies with central surface brightness $\mu_{0,V} \approx 23$ mag arcsec^{-2}, where the slope of the $M_V - \mu_{0,V}$ relation changes, have nearest neighbour distances scattering between 20 and 300 kpc. However, they all have luminosities $M_V \approx -14$ mag. From this exercise, we can conclude that the photometric scaling relations presented in Fig. 2 are not a consequence of environmental segregation, with fainter galaxies preferentially located close to a bright galaxy.

Park & Choi (2008) study the structural parameters such as the concentration index, Petrosian radius, velocity dispersion, $u - r$ colour, . . ., of a volume-limited sample of 49 571 galaxies extracted from the Sloan Digital Sky Survey (SDSS). They show that these parameters are almost independent of large-scale density and neighbour separation unless the latter is smaller than about one-tenth of the bright neighbour's virial radius, i.e. of the order of a few tens of kpc (their figs 7 and 9). All galaxies presented in the present paper have projected distances between 0.1 and 1 virial radii away from their nearest bright neighbour and, as Park & Choi (2008), we observe no significant relation between nearest-neighbour distance or environment density and structural properties in this regime. This also corroborates the results of Weinmann et al. (2008) who study a sample of galaxies selected from the SDSS DR4 and find that the structural properties of early-type satellite galaxies are very similar to early-type central galaxies. Hence, the structure of early-type galaxies is not significantly affected by environmental effects.

The most obvious environmental effect appears to be the population of low surface brightness dSphs discovered by Mieske et al. (2007) in the Fornax cluster. Where an environmental influence is clearly discernible, it has only mild effects on the scaling relations. The presence of a low surface brightness population of the Fornax dSphs does not affect the global scaling relation appreciably. At a given luminosity, the Fornax dSph population is on average 0.2 mag arcsec^{-2} fainter than the Perseus and Local Group dSph populations. The M31 companions with tidal extensions or distorsions (Lewis et al. 2007; Ségall et al. 2007) are not displaced from the general scaling relations. This may indicate that the dSphs intrinsically have high-enough M/L to survive unscathed (see Penny et al. 2008) or that dSphs with too low M/L have been destroyed and only those with high M/L survive to the present day.

ACKNOWLEDGMENTS

SDR wishes to thank Philippe Prugniel and Mina Koleva for their hospitality and for the stimulating discussions while visiting CRAL

Lyon Observatory during the course of this work. CJC and SJP acknowledge support from STFC. SDR is a Postdoctoral Fellow of the Fund for Scientific Research – Flanders (Belgium)(FWO). SV is a PhD Fellow of the Fund for Scientific Research – Flanders (Belgium)(FWO). This research has made use of the NASA/IPAC Extragalactic Data base (NED) which is operated by the Jet Propulsion Laboratory, California Institute of Technology, under contract with the National Aeronautics and Space Administration.

REFERENCES

Bender R., Surma P., Döbereiner S., Möllenhoff C., Madejsky R., 1989 A&A, 217, 35
Blitz L., Robishaw T., 2000, ApJ, 541, 675
Buyle P., De Rijcke S., Michielsen D., Baes M., Dejonghe H., 2005, MNRAS, 360, 853
Caldwell N., 1999, AJ, 118, 1230
Carraro G., Chiosi C., Girardi L., Lia C., 2001, MNRAS, 335, 335
Conselice C. J., 2003, ApJS, 147, 1
Conselice C. J., Gallagher J. S. III, Wyse R. F. G., 2003a, AJ, 125, 66
Conselice C. J., O'Neil K., Gallagher J. S., Wyse R. F. G., 2003b, ApJ, 591, 167
Couture J., Harris W. E., Allwright J. W. B., 1990, ApJS, 73, 671
De Rijcke S., Zeilinger W. W., Dejonghe H., Hau G. K. T., 2003, MNRAS, 339, 225
De Rijcke S., Michielsen D., Dejonghe H., Zeilinger W. W., Hau G. K. T., 2005, MNRAS, 360, 853 (D05)
De Rijcke S., Prugniel P., Simien F., Dejonghe H., 2006, MNRAS, 369, 1321
De Rijcke S., Zeilinger W. W., Hau G. K. T., Prugniel P., Dejonghe H., 2007, ApJ, 659, 1172
Goto T., Yamauchi C., Fujita Y., Okamura S., Sekiguchi M., Smail I., Bernardi M., Gomez P. L., 2003, MNRAS, 346, 601
Gourgoulhon E., Chamaraux P., Fouqué P., 1992, A&A, 255, 69
Graham A. W., Guzmán R., 2003, AJ, 126, 1787 (GG03)
Graham A. W., Worley C. C., 2008, MNRAS, 388, 1708
Grebel E. K., Gallagher J. S. III, Harbeck D., 2003, AJ, 125, 1926
Held E. V., de Zeeuw T., Mould J., Picard A., 1992, AJ, 103, 851
Irwin M., Hatzidimitriou D., 1995, MNRAS, 277, 1354
Jerjen H., 2003, A&A, 398, 63
Jerjen H., Binggeli B., 1997, in Arnaboldi M. A., Da Costa G. S., Saha P., eds, ASP Conf. Series, Vol. 116, 2nd Stromlo Symposium, The Nature of Elliptical Galaxies, Astron. Soc. Pac., San Francisco, p. 239
Johnston K. V., Spergel D. N., Hernquist L., 1995, ApJ, 451, 598
Kleyna J. T., Wilkinson M. I., Evans N. W., Gilmore G., 2005, ApJ, 630, L141
Kundu A., Whitmore B. C., 1998, AJ, 116, 2841
Lewis G. F., Ibata R. A., Chapman S. C., McConnachie A., Irwin M. J., Tolstoy E., Tanvir N. R., 2007, MNRAS, 375, 1364
Lisker T., Glatt K., Westera P., Grebel E. K., 2006, AJ, 132, 2432
Łokas E. L., 2002, MNRAS, 333, 697
Marcolini A., Brighenti F., D'Ercole A., 2003, MNRAS, 345, 1329
Marcolini A., D'Ercole A., Brighenti F., Recchi S., 2006, MNRAS, 371, 64
Martin N. F., de Jong T. A., Rix H.-W., 2008, ApJ, 684, 1075
Mateo M. L., 1998, ARA&A, 36, 435
Mateo M., Mirabal N., Udalski A., Szymanski M., Kaluzny J., Kubiak M., Krzeminski W., Stanek K. Z., 1996, ApJ, 458, L13
Mateo M., Olszewski E. W., Walker M. G., 2008, ApJ, 675, 201
Matković A., Guzmán R., 2005, MNRAS, 362, 289
McConnachie A. W., Irwin M. J., 2006, MNRAS, 365, 1263
McConnachie A. W., Arimoto N., Irwin M., 2007, MNRAS, 379, 379
Michielsen D. et al., 2007, ApJ, 670, L101
Mieske S., Hilker M., Infante L. M. C., 2007, A&A, 463, 503
Nagashima M., Yoshii Y., 2004, ApJ, 610, 23
Park C., Choi Y.-Y., 2008, ApJ, preprint (arXiv:0809.2156)
Peletier R. F., 1993, A&A, 271, 51
Penny S. J., Conselice C. J., 2008, MNRAS, 383, 247
Penny S. J., Conselice C. J., De Rijcke S., Held E. V., 2008, MNRAS, in press (arXiv:0811.3197)
Prugniel P., Simien F., 1997, A&A, 321, 111
Ricotti M., Gnedin N. Y., 2005, ApJ, 629, 259
Saviane I., Held E. V., Piotto G., 1996, A&A, 315, 40
Schlegel D. J., Finkbeiner D. P., Davis M., 1998, ApJ, 500, 525
Ségall M., Ibata R. A., Irwin M. J., Martin N. F., Chapman S., 2007, MNRAS, 375, 831
Sharina M. E. et al., 2008, MNRAS, 384, 1544
Sirianni M. et al., 2005, PASP, 117, 1049
Smith Castelli A. V., Bassino L. P., Richtler T., Cellone S. A., Aruta C., Infante L., 2008, MNRAS, 386, 2311
Struble M. F., Rood H. J., 1999, ApJS, 125, 36
Tonry J. L., Dressler A., Blakeslee J. P., Ajhar E. A., Fletcher A. B., Luppino G. A., Metzger M. R., Moore C. B., 2001, ApJ, 546, 681
Valcke S., De Rijcke S., Dejonghe H., 2008, MNRAS, 389, 1111
van Zee L., Barton E. J., Skillman E. D., 2004, AJ, 128, 2797
Vazdekis A., Casuso E., Peletier R. F., Beckman J. E., 1996, ApJS, 106, 307
Weinmann S. M., Kauffmann G., van den Bosch F. C., Pasquali A., McIntosh D. H., Mo H., Yang X., Guo Y., 2008, MNRAS, preprint (arXiv0809.2283)
Young L. M., Skillman E. D., Weisz D. R., Dolphin A. E., 2007, ApJ, 659, 331
Zucker D. B., Kniazev A. Y., Martínez-Delgado D., Bell E. F., Rix H.-W. et al., 2007, ApJ, 659, L21

This paper has been typeset from a TEX/LATEX file prepared by the author.